Revealing heterogeneity of brain imaging phenotypes in Alzheimer's disease based on unsupervised clustering of blood marker profiles

Gerard Martí-Juan[1*], Gerard Sanroma[2], Gemma Piella[1], for the Alzheimer's Disease Neuroimaging Initiative and the Alzheimer's Disease Metabolomics Consortium ˆ

1 BCN Medtech, Department of Information and Communication Technologies, Universitat Pompeu Fabra, Barcelona

2 German Center for Neurodegenerative Diseases (DZNE), Bonn, Germany

ˆ Data used in preparation of this article were obtained from the Alzheimer's Disease Neuroimaging Initiative (ADNI) database (`adni.loni.usc.edu`) and generated by the Alzheimer's Disease Metabolomics Consortium (ADMC). As such, the investigators within the ADNI and the MDMC contributed to the design and implementation of ADNI and/or provided data but did not participate in analysis or writing of this report. A complete listing of ADNI investigators can be found at: `http://adni.loni.usc.edu/wp-content/uploads/how_to_apply/ADNI_Acknowledgement_List.pdf`, and a complete listing of ADMC investigators can be found at: `https://sites.duke.edu/adnimetab/about-us/the-team/`.

* gerard.marti@upf.edu (GM)

Abstract

Alzheimer's disease (AD) affects millions of people and is a major rising problem in health care worldwide. Recent research suggests that AD could have different subtypes, presenting differences in how the disease develops. Characterizing those subtypes could be key to deepen the understanding of this complex disease. In this paper, we used a multivariate, non-supervised clustering method over blood-based markers to find

subgroups of patients defined by distinctive blood profiles. Our analysis on ADNI database identified 4 possible subgroups, each with a different blood profile. More importantly, we show that subgroups with different profiles have a different relationship between brain phenotypes detected in magnetic resonance imaging and disease condition.

Author summary

Alzheimer's disease (AD) degenerates the brain and causes cognitive deterioration and loss of memory, leading to death. It is one of the largest problems in public health in the world, and while many efforts have been inverted into studying it, many things about the disease are still unknown. One of the open questions is whether there are various subtypes of the disease. Does the disease behave differently between patients? If so, why? In this work we try to answer this question by using markers found in the blood, easily gathered with inexpensive, non-invasive methods, to identify different presentations of the disease where it interacts differently with the brain. We use a machine learning approach to process large amounts of data and detect possible hidden relationships between the markers. Our results show promising differences in interactions between the disease and brain degeneration depending on the found blood profiles.

Introduction

Alzheimer's disease (AD) is the most common cause of dementia, a condition affecting more than 47 million people worldwide [1]. AD is one of the biggest concerns in global health care, due to its large economic and social impact. It is characterized by a deposition of amyloid-beta (Aβ) protein in the brain and the formation of tau plaques [2], and its most prevalent symptom is a progressive decline and deterioration of cognitive skills, leading to death. AD has been characterized as a multi-factorial disease [2, 3], involving many different processes and biological phenomena. Despite many efforts spent on research, we know relatively little about many aspects of the disease.

Currently, to accurately diagnose the disease and provide for an adequate treatment, several markers are used: cerebrospinal fluid (CSF) concentration of tau, p-tau and Aβ [4], and markers obtained from imaging techniques such as magnetic resonance imaging (MRI) to detect structural neurodegeneration, or positron emission tomography (PET) to detect Aβ concentration and tau deposition in the brain [5, 6]. Efforts have been made to find new, less-invasive markers in blood that can help diagnose the disease. In 2009, Schneider et al. [7] presented a review of proposed plasma marker candidates, concluding that a single reliable candidate had not been found yet. O'Bryant et al. [8], in their review on blood-based markers for AD detection, concluded that, while progress has been made, significant advancements on results validation are still needed before blood markers can be reliably used in clinical trials.

Several blood markers have been shown to correlate with structural changes. Dage et al. [9] studied the connection between neurodegeneration and tau protein levels in plasma, finding association between cortical thickness, cognition, and tau levels. In a study by Mattsson et al. [10], plasma neurofilament light was associated with cognitive deterioration and imaging markers of AD. Thambisetty et al. [11] analyzed the relationship between various plasma proteins and brain volume in AD patients, finding links between plasma proteins and AD neurodegeneration. In a later work [12], they studied the relationship between plasma clusterin (apolipoprotein J) concentration and longitudinal brain atrophy, finding significant associations.

These previous described works do not take into account the possible heterogeneity arising from the interaction between blood and brain. AD is a highly heterogeneous disease, where its symptoms and path of degeneration can vary between patients, and identifying the different presentations or subtypes and their related signatures could help for a better detection of the disease and a better understanding of the interaction between different biological mechanisms (i.e. phenotypes). There have been many studies identifying possible heterogeneous subgroups of the disease. Noh et al. [13] found 3 subtypes on distinct patterns of cortical atrophy, using Ward's clustering linkage method. Nettiksimmons et al. [14] presented subtypes based on CSF and MRI markers, and in a posterior study [15], they argued that vascular damage could explain subtyping difference. They also studied heterogeneity in mild cognitive impairment patients [16], using CSF, MRI, and plasma markers. In a different approach, Young et

al. [17, 18] proposed an event ordering method to infer heterogeneous subtypes of the disease and stage.

Heterogeneity studies generally use the same data modality to both subtype the disease and analyze the obtained subgroups. This could hide relevant differences from other modalities. Moreover, clustering over features that are strongly correlated to the disease stage could lead to subgroups divided by disease severity, instead of by possible disease subtypes. Instead, we propose use blood marker features to define the subgroups and then explore the relationships with the disease in each subgroup using brain volume phenotypes and disease stages. We use a data-driven, non-supervised, multivariate clustering technique [19] to identify different presentations of the disease using blood markers, and then we analyze how the different blood profiles interact with brain structural phenotypes across the different disease stages. Compared to methods limited by univariate analysis, such as direct statistical tests for a single marker, multivariate analysis allows us to identify possible hidden blood marker profiles associated with latent pathological processes, addressing a limitation of the reported blood marker studies.

Materials and methods

Data

Data from the Alzheimer's Disease Neuroimaging Initiative (ADNI) database (`adni.loni.usc.edu`) was used for this project. ADNI is a multi-site, longitudinal study launched in 2003 by Weiner et al. [20] that includes acquisitions of MRI, PET, other biological markers, and clinical and neuropsychological assessment tests of patients over time to track the pathology of AD. For this work, we have selected subjects that had available MRI T1.5 scan and blood marker information at baseline. After removing subjects that presented missing values, we ended up with a set of 298 subjects, including 52 cognitive normal (CN), 161 with mild cognitive impairment (MCI) and 85 with AD. Table 1 shows the demographic information of the studied cohort.

172 plasma markers were selected from the available cohort of markers in ADNI, taking into account the reported quality of the samples and removing any marker that had missing values. MRI data was processed and registered to a common space using

	CN	MCI	AD	Total
Nº subjects	52	161	85	298
Age (years)	75.13 ± 5.99	74.15 ± 7.51	74.57 ± 7.95	74.4 ± 7.39
Gender (female)	44.2%	33.5%	47%	39.3%
Education (years)	15.85 ± 2.75	15.844 ± 2.95	15.29 ± 2.98	15.68 ± 2.75
Apoe4 (+)	9%	52%	67%	48%
MMSE	29 ± 1.19	26.97 ± 1.78	23.45 ± 1.96	26.32 ± 2.62

Table 1. Demographic information of the studied cohort. Categorical variables are expressed as counts and percentages. Continuous variables are expressed as mean ± standard deviation. MMSE = mini-mental state examination.

Freesurfer's *recon-all* [21]. We selected 39 volumes of structures from relevant subcortical regions of the brain defined in the default atlas of Freesurfer [22] for interaction analysis. A full list of the selected plasma markers and brain regions can be found in S1 data. Each volume value was normalized by the estimated intracraneal volume (eTIV) of the subject. Data (both structural volumes and blood markers) were transformed to $[0, 1]$ range before processing.

Methods

To find the different profiles, we cluster the patients using their blood markers, without using neither brain phenotypes nor diagnosis. We analyze the resulting clusters to find the blood profiles of each cluster. To find heterogeneous brain presentations in each cluster, we analyze the relationships between brain phenotypes in each cluster and disease stage, thus revealing the interactions between blood marker profiles and brain phenotypes across the disease stages. Fig 1 shows the pipeline of the method.

Fig 1. Method overview. We detect clusters on the space defined by the blood markers, define a different profile for each cluster, and, using the phenotypes extracted from the MRI images, we analyze the interactions between the profiles and the disease.

Unsupervised clustering

We use CIMLR [19, 23] to identify the blood markers that reveal natural subgroups in the data, without taking into account neither the brain phenotypes nor the disease stage, to obtain subtypes not defined by disease stage. We could have used any other unsupervised clustering method, but we selected CIMLR, coupled with manifold

learning and k-means clustering, due to its scalability with large amounts of data, good performance on a variety of datasets [19, 23], and interpretability of results.

CIMLR is a method based on multiple kernel learning (MKL) that learns a similarity between each pair of samples by combining different kernels per feature (in our case, blood markers). It enforces a C block structure on the learned similarity, where each block is a set of samples similar to each other, i.e., a cluster. The number of clusters C must be specified beforehand. The learned similarity can then be used to compute a space of reduced complexity, where each subject is positioned with respect to the whole population, and the distance between subjects indicates how similar they are. By combining multiple kernels, each of which is based on a specific blood marker, it integrates the heterogeneous information, and provides the contribution of each blood marker in the computed low-dimensional representation.

Let the input data consist of N samples with M features (i.e., blood markers) each, be defined as $\{x_{im}\}_{i=1}^{N}$, $m = 1, \ldots, M$, where x_{im} represents the blood marker m of subject i. Each blood marker is assigned to P kernels K_{mp}, $p = 1, \ldots, P$. CIMLR solves for 3 variables: $S \in \mathbb{R}^{N \times N}$ (the learned similarity matrix), $w \in \mathbb{R}^{M \cdot P \times 1}$ (a vector containing the weights associated to each kernel), and $A \in \mathbb{R}^{N \times C}$ (a matrix enforcing C clusters in S). The optimization problem is defined as follows:

$$\begin{aligned} \min_{S,A,w} - \sum_{i,j,p,m} w_{mp} K_{mp}(x_{im}, x_{jm}) S_{ij} + \gamma tr(A^T (I_N - S) A) \\ + \mu \sum_{m,p} w_{mp} \log\, w_{mp} + \beta \|S\|_F^2 \\ \text{subject to } A^T A = I_C, \sum_{m,p} w_{mp} = 1, w_{mp} \geq 0, \sum_j S_{ij} = 1 \text{ and } S_{ij} \geq 0. \end{aligned} \tag{1}$$

Here, $\gamma, \mu,$ and β are tuning parameters for the various terms of the optimization function, I represents the identity matrix, $\|.\|_F$ stands for the Frobenius norm, and tr denotes the trace of the matrix. The first term of Equation 1 links the learned similarity S with the combination of kernels from all features: similarity between two samples should be small if their kernel-based distance is large. The second term enforces S to have C connected components, through the auxiliary matrix A and its associated constraint I_C. The third term imposes a constraint on w so that more than one kernel

is selected, and last term applies a regularization penalizing the scale of the learned similarities. An extended overview of the algorithm, including the optimization method, can be found in [19]. A MATLAB implementation of the method by the authors of the paper has been used (`https://github.com/BatzoglouLabSU/SIMLR`).

We use Gaussian kernels to define K_{mp}. In total, there are P kernels for each feature m, each with different parameters. This is needed because different markers could be sensitive to different ranges of parameters. We define K_{mp} as:

$$\begin{aligned} K_{mp}(x_i, x_j) &= \frac{1}{\epsilon_{ijp}\sqrt{2\pi}} \exp\left(-\frac{\|x_{im} - x_{jm}\|_2^2}{2\epsilon_{ijm}^2}\right), \\ \mu_{im} &= \frac{\sum_{j \in KNN(x_{im})} \|x_{im} - x_{jm}\|_2}{k}, \epsilon_{ijm} = \frac{\sigma(\mu_{im} + \mu_{jm})}{2}, \end{aligned} \tag{2}$$

with $KNN(x_{im})$ representing the k nearest neighbours of subject i with respect to marker m, and $\|.\|_2$ being the Euclidean distance. For $k \in \{30, 45, 50\}$ and $\sigma \in \{30, 35, 40, 45, 50\}$, we have a total of $P = 15$ kernels for each feature. The choice of parameters was done empirically. The method is mainly invariable to P [23]. For 172 markers, we optimize over a total of $15 \times 172 = 2580$ kernels.

As in [19], we estimate the best number of clusters with the heuristic proposed in [24], and further validate the choice with the elbow method. For visualization of the clusters and dimensionality reduction, we apply t-SNE [25], a manifold learning technique, on the resulting similarity matrix. After obtaining the low dimensional embedding, k-means clustering is used to discover the clusters.

Cluster validation

We want to test the stability of the clusters against perturbations (e.g. particular choice of individuals). If the same clusters arise after modifying the choice of individuals, this points that the clustering is capturing an underlying structure in the data that is invariant to the particular choice of individuals, to some extent. We use a bootstrap procedure to test this stability. We apply the CIMLR-based clustering method to randomly select subsets of the data, with the same size of the original dataset but with replacement (i.e. some patients could appear several times, while others could not appear at all). After applying the clustering algorithm, we compute the similarity of the

obtained clusters in each bootstrap iteration with the clusters obtained for the whole dataset.

We use the Jaccard index to quantify the similarity between clusters. This Jaccard index is defined, for two sets A, B, as the intersection divided by the union of the sets:

$$J(A,B) = \frac{|A \cap B|}{|A \cup B|} = \frac{|A \cap B|}{|A| + |B| - |A \cap B|}. \tag{3}$$

The higher the index, the higher the similarity and hence the stability.

Profile discovery

Subjects in a given cluster share a specific profile of blood markers. To obtain the profile of each cluster, we need to determine which markers contributed more to the clustering. We look at the weights w in the optimization procedure: each weight accounts for the importance of a specific kernel. As described above, we generate 15 kernels for each of the 172 markers, with 15 associated weights. We compute the importance as the sum of those weights.

For further validation, we use one-way ANOVA tests of mean population across the clusters for the described markers to test whether the population of each subtype has a different mean. With this, we obtain a stable list of the most informative markers for the clustering, and describe the different blood profiles in each subgroup according to that set of markers.

Interaction analysis

To detect different interactions between blood markers and structural brain phenotypes, we tested for differences between the brain volumes of the individuals in each subgroup. We used a non-parametric Mann-Whitney-Wilcoxon test. We performed three different comparison tests:

1. **Whole cluster analysis:** Each subgroup and the rest of the population, not taking into account diagnostic groups, to detect different characteristics in each subgroup.

2. **Diagnosis group analysis:** Diagnostic groups, for each subgroup, to find

differences between stages of the disease in each subgroup with respect to the whole population.

3. **Diagnosis interaction analysis:** Each diagnostic group of each subgroup with the rest of subjects on the population in that diagnostic group, to detect different interactions between blood profiles and structural brain phenotypes across different stages of the disease.

Fig 2. Permutation procedure. For groups G1 and G2, we create new random subgroups and test them. Then, we corrected the obtained result in the original group (P_c, red line), with respect to the 5% percentile of the obtained distribution of p-values ($P_{0.05}$, black line). If the result is in the percentile, we consider it significant.

We want to know whether cluster membership (independent variable) has significant effects on brain volume (dependent variable). The significance thresholds may vary depending on the samples sizes, especially in our case that the groups may have different number of samples (i.e. clusters of different size). To correct for different sized groups and remove false positives, we used a permutation based method [26]. For a large enough number of iterations (1000), we perform random permutation of the independent variable (i.e. cluster membership), while preserving the cluster sizes and the diagnostic group sizes. This way, we obtain a distribution of significance values.

According to the permutation strategy and for the test to be significant, we must have a higher significance than that of most of the random permutations (e.g. 95%, 99%, ... depending on the desired significance level). This correction is done to ensure that the obtained statistical significance was not caused by the different sample sizes of each subgroup and each diagnostic group. Fig 2 shows an outline of the procedure.

Results

We applied the proposed method to the described cohort of subjects from ADNI database, to find the subgroups with heterogeneous blood profiles and analyze the interactions with the disease of each subgroup using volume features. All the experiments are reproducible following the instructions found in the repository of the project `https://github.com/GerardMJuan/simlr-ad`.

Clustering

After applying the heuristics on cluster size described in the Methods section, we obtained $C \in \{4, 6\}$ using [24] and $C \in \{4, 5\}$ using the elbow method. We decided on $C = 4$ as the most appropriate choice. Figure 3 shows the learned similarity matrix S and the cluster distribution in the first two dimensions of the low-dimensional space identified by t-SNE. We compared it to the similarity matrix and cluster distribution obtained using Euclidean distance on the original blood marker space. Fig 3 illustrates that clusters are not distinguishable when using an Euclidean-based similarity matrix, while CIMLR has a block structure that improves dimensionality reduction and cluster analysis.

Fig 3. Similarity matrices and 2D embeddings a) Euclidean distance between subjects over the initial blood marker space. b) Learnt similarity matrix S. Subjects in the matrix are ordered by the obtained clusters. c) d) 2D embeddings of the respective matrices in a) and b) using t-SNE.

We assessed the stability of the obtained clusters by using the bootstrap approach described in the Methods section and compared it with stability results obtained using a random clustering and k-means clustering with Euclidean metric. Table 2 shows the results. CIMLR got a larger mean similarity in each cluster than random clustering, and similar stability to k-means clustering. Clusters C1 and C2 appeared more stable than C3 and C4.

Cluster	Random	k-means	CIMLR
C1	0.227	0.453	0.467
C2	0.208	0.435	0.409
C3	0.187	0.320	0.317
C4	0.206	0.331	0.386

Table 2. Stability tests for the clustering, compared to random clustering and k-means clustering using Euclidian distance. Reported result is mean similarity.

Table 3 shows the demographic information of the subjects for each obtained cluster. Distribution of the diagnosis groups is similar to the distribution in the whole population, and the other characteristics (age, gender, education, Mini–Mental State Examination results (MMSE) and APoe4 genotype) are also similar across subgroups, with the exception of the mean age of C4, which is 5 years lower than the mean

population, and a slightly higher amount of women in C3 and C4. No major significant differences between subgroups were observed, meaning that the obtained groups were not biased.

	Total	C1	C2	C3	C4
N subj	298	82	77	61	78
CN	52	17	15	12	8
MCI	161	35	44	33	49
AD	85	30	18	16	21
Age	74.45 ± 7.39	77.25 ± 6.94	75.59 ± 6.12	75.09 ± 7.14	69.87 ± 7.22
Gender	39%	25%	28%	52%	53%
Education	15.69 ± 2.92	15.90 ± 2.57	14.99 ± 3.42	15.57 ± 2.47	16.24 ± 2.98
APoe4	48%	37%	54%	45%	57%
MMSE	26.33 ± 2.62	25.90 ± 2.95	26.65 ± 2.37	26.25 ± 2.73	26.51 ± 2.38

Table 3. Demographic characteristics of the different clusters. Categorical variables are expressed as counts and percentages. Continuous variables are expressed as mean $\pm$ standard deviation.

Blood marker ranking and profiling

CIMLR revealed patterns of blood markers that relate to natural subgroups. Fig 4 shows the ten most relevant markers determined by the weight vector w. The method uses all blood markers to find the clusters but, unlike other methods, it automatically weights each marker. S4 data contains the full set of weights.

Fig 4. Marker weights. Top 10 marker weights in the kernel combination.

Fig 5 shows the values for each marker and cluster. All the ANOVA tests done for each of the described markers reject the null hypothesis with $p < 0.0001$, meaning that the differences found between clusters on those blood markers are statistically significant.

Fig 5. Marker distributions. Distribution of top ten ranked markers for each cluster. Normalized values.

Each of the profiles is defined by different values of the markers:

- C1 presents larger concentrations of B2M, Cystatin-C and lower THBS1 with respect to the total population.
- C2 shows decreased values in all of the relevant markers compared to the whole population, with the exception of B2M.

- C3 shows higher values in all of the relevant markers compared to the whole population, with the exception of B2M and Cystatin-C.
- C4 presents lower values of B2M, Cystatin-C and higher values of every other marker, compared with the general population.

It is interesting the absence of tau and amyloid-related markers, which are associated with dementia [9, 27, 28]. However, as per table 3, we know that the defined subgroups have a diagnostic distribution similar to the whole population: if markers that were highly correlated to the disease stage (such as the tau and amyloid related markers) had been selected by the algorithm, then that distribution would have been biased.

Interaction analysis

We analyzed the heterogeneity between the different groups and the interactions between the stages of the disease and the brain volume phenotypes depending on the blood profiles in each subgroup, as described in the Methods section.

Whole cluster analysis

We compared brain volumes in each subgroup against the rest of the population, corrected for different group sizes and false positives using permutation tests. Fig 6 shows the differences in the characteristics of the population in each subgroup. C1 presents significant differences in the ventricles, putamen, accumbens area, left-vessel, right-pallidum, choroid plexus and posterior corpus callosum. C2 and C3 are similar to the general population: C2 only shows differences in the corpus callosum central and anterior, while C3 is only different to the rest in the right accumbens area. C4 shows many differences in the choroid plexus, ventricles, putamen and pallidum, among others.

Fig 6. Whole cluster analysis. Differences in volume for each subgroup population against the rest. Corrected using permutation.

Diagnosis group analysis

To identify differences between diagnosis groups in each of the subgroups, we compared between diagnosis groups (CN, MCI, AD) for each of the different subgroups (C1 to C4). In this task, permutation tests allows us to detect differences between diagnosis groups that are specific to that subgroup, by correcting the result against random subgroups. Figs 7-8 show the difference between diagnosis groups in: (i) each of the subgroups (Fig 7) and (ii) the whole population (Fig 8).

Fig 7. Diagnosis group analysis. Differences between diagnosis stage groups for each of the presentations. Corrected using permutation.

Fig 8. Diagnosis group analysis, whole population. Differences between diagnosis stage groups on the whole population.

There are significant differences in C3 between CN and AD subjects in the corpus callosum, the third ventricle and the choroid plexus, and in C4 between CN and MCI subjects in the corpus callosum and the ventricles. C1 and C2 have more sparse differences with respect to the whole population.

Most of the statistically significant differences correspond to volumes that show less significant differences on the whole population analysis. Intra-group heterogeneity between disease stages is located in specific regions that are usually less affected by the disease.

Diagnosis interaction analysis

To detect different interactions between blood profiles and brain phenotypes across different stages of the disease, we tested for differences across same diagnosis subgroups for each cluster against the rest of the population with the same diagnosis. Fig 9 shows the results.

Fig 9. Diagnosis interaction analysis. Differences between diagnosis stages across presentations. Corrected using permutation.

We observed differences in volume across all the subgroups:

- C1 differs in AD, presenting differences in cerebellum, white matter and left pallidum volume. CN and MCI subgroups do not present differences in interaction compared to the whole population.

- C2 presents differences in all three subgroups, showing differences in the amygdala for CN patients, and strong differences in the vessels for the AD subgroups, among others.

- C3 shows many differences in the CN patients, in the right putamen, caudate, amygdala and accumbens. It also differs in the AD interaction in the cerebellum white matter volume.

- C4 shows differences in MCI and AD subgroups, in the amygdala, accumbens, corpus callosum and others for MCI, and right vessel, CSF and optic chiasm in the AD subgroup.

Those differences suggest that the interactions between the disease and the brain volumes could be different depending on the blood presentations of each subgroup.

Discussion

We applied a multivariate data-driven procedure for AD subtyping using blood-based markers, to obtain heterogeneous groups with different blood profiles. We showed that patients with different profiles present different interactions between disease stage and brain phenotypes. While existing blood markers can still not be used to properly diagnose the disease [7, 29, 30], using blood markers to detect patient profiles where the disease could behave differently and could provide valuable biological insights is a promising research direction.

The method identifies natural subgroups of patients in a multivariate way, finding hidden associations between the markers and automatically weighting the most important ones. The method is scalable to a large number of subjects and to a large number of features, allowing for an easier incorporation of other types of data, such as genotypes or other not-included blood markers. It also has some limitations: the obtained subgroups do not have a high stability. We also did not compare to other possible subtyping methods to further validate the obtained results.

From a clinical point of view, a clinical study of the detected profiles is needed to study possible implications of the found markers. Further validation of the results on a larger, independent cohorts of patients will be important to confirm the results and

detect more complex profiles. Interactions of the profiles could also be further validated in other phenotypes, such as longitudinal brain atrophy or cortical thickness.

Supporting information

S1 File. PTID list. List of Patient ID (PTID) of the ADNI subjects used in this study.

S2 File. Volumes List. List of subcortical zones from Freesurfer segmentation used in this study.

S3 File. Blood markers list. List of blood markers available in the ADNI website used in this study.

S4 File. Full set of weights. List of the weights assigned to each blood marker during computation.

Acknowledgments

Data collection and sharing for this project was funded by the Alzheimer's Disease Neuroimaging Initiative (ADNI) (National Institutes of Health Grant U01 AG024904) and DOD ADNI (Department of Defense award number W81XWH-12-2-0012). This research was partially funded by the "Fundació La Marató de TV3" (nº20154031).

References

1. Alzheimer's Association . Alzheimer's & Dementia: Global Resources;. Available from: `https://www.alz.org/global/`.

2. Jack CR, Bennett DA, Blennow K, Carrillo MC, Dunn B, Haeberlein SB, et al. NIA-AA Research Framework: Toward a biological definition of Alzheimer's disease. Alzheimer's & Dementia. 2018;14(4):535–562. doi:10.1016/j.jalz.2018.02.018.

3. Jack CR, Knopman DS, Jagust WJ, Petersen RC, Weiner MW, Aisen PS, et al.. Tracking pathophysiological processes in Alzheimer's disease: An updated hypothetical model of dynamic biomarkers; 2013.

4. Andreasen N, Minthon L, Vanmechelen E, Vanderstichele H, Davidsson P, Winblad B, et al. Cerebrospinal fluid tau and Aβ42 as predictors of development of Alzheimer's disease in patients with mild cognitive impairment. Neuroscience Letters. 1999;273(1):5–8. doi:10.1016/S0304-3940(99)00617-5.

5. Weiner M, Khachaturian Z. The Use of MRI and PET for Clinical Diagnosis of Dementia and Investigation of Cognitive Impairment: A Consensus Report. Alzheimer's Association, Chicago, IL. 2005;(1):1–15.

6. Clark CM, Schneider JA, Bedell BJ, Beach TG, Bilker WB, Mintun MA, et al. Use of florbetapir-PET for imaging β-amyloid pathology. JAMA - Journal of the American Medical Association. 2011;305(3):275–283. doi:10.1001/jama.2010.2008.

7. Schneider P, Hampel H, Buerger K. Biological Marker Candidates of Alzheimer's Disease in Blood, Plasma, and Serum. CNS Neuroscience & Therapeutics. 2009;15(4):358–374. doi:10.1111/j.1755-5949.2009.00104.x.

8. O'Bryant SE, Mielke MM, Rissman RA, Lista S, Vanderstichele H, Zetterberg H, et al. Blood-based biomarkers in Alzheimer disease: Current state of the science and a novel collaborative paradigm for advancing from discovery to clinic. Alzheimer's and Dementia. 2017;13(1):45–58. doi:10.1016/j.jalz.2016.09.014.

9. Dage JL, Wennberg AMV, Airey DC, Hagen CE, Knopman DS, Machulda MM, et al. Levels of tau protein in plasma are associated with neurodegeneration and cognitive function in a population-based elderly cohort. Alzheimer's and Dementia. 2016;12(12):1226–1234. doi:10.1016/j.jalz.2016.06.001.

10. Mattsson N, Andreasson U, Zetterberg H, Blennow K. Association of Plasma Neurofilament Light With Neurodegeneration in Patients With Alzheimer Disease. JAMA neurology. 2017;74(5):557–566. doi:10.1001/jamaneurol.2016.6117.

11. Thambisetty M, Simmons A, Hye A, Campbell J, Westman E, Zhang Y, et al. Plasma biomarkers of brain atrophy in Alzheimer's disease. PLoS ONE. 2011;6(12):e28527. doi:10.1371/journal.pone.0028527.

12. Thambisetty M, An Y, Kinsey A, Koka D, Saleem M, Guntert A, et al. Plasma clusterin concentration is associated with longitudinal brain atrophy in mild cognitive impairment. NeuroImage. 2012;59(1):212–217. doi:10.1016/j.neuroimage.2011.07.056.

13. Noh Y, Jeon S, Lee JM, Seo SW, Kim GH, Cho H, et al. Anatomical heterogeneity of Alzheimer disease Based on cortical thickness on MRIs. Neurology. 2014;83(21):1936–1944. doi:10.1212/WNL.0000000000001003.

14. Nettiksimmons J, Harvey D, Brewer J, Carmichael O, DeCarli C, Jack CR, et al. Subtypes based on cerebrospinal fluid and magnetic resonance imaging markers in normal elderly predict cognitive decline. Neurobiology of Aging. 2010;31(8):1419–1428. doi:10.1016/j.neurobiolaging.2010.04.025.

15. Nettiksimmons J, Beckett L, Schwarz C, Carmichael O, Fletcher E, DeCarli C. Subgroup of ADNI normal controls characterized by atrophy and cognitive decline associated with vascular damage. Psychology and Aging. 2013;28(1):191–201. doi:10.1037/a0031063.

16. Nettiksimmons J, DeCarli C, Landau S, Beckett L. Biological heterogeneity in ADNI amnestic mild cognitive impairment. Alzheimer's & dementia : the journal of the Alzheimer's Association. 2014;10(5):511–521. doi:10.1016/j.jalz.2013.09.003.

17. Young AL, Oxtoby NP, Huang J, Marinescu RV, Daga P, Cash DM, et al. Multiple Orderings of Events in Disease Progression for the Alzheimer's Disease Neuroimaging Initiative;.

18. Young AL, Marinescu RV, Oxtoby NP, Bocchetta M, Yong K, Firth N, et al. Uncovering the heterogeneity and temporal complexity of neurodegenerative diseases with Subtype and Stage Inference. bioRxiv. 2017; p. 236604. doi:10.1101/236604.

19. Ramazzotti D, Lal A, Wang B, Batzoglou S, Sidow A. Multi-omic tumor data reveal diversity of molecular mechanisms underlying survival. bioRxiv. 2018; p. 267245. doi:10.1101/267245.

20. Mueller SG, Weiner MW, Thal LJ, Petersen RC, Jack C, Jagust W, et al.. The Alzheimer's disease neuroimaging initiative; 2005.

21. Fischl B. FreeSurfer; 2012.

22. Fischl B, Salat DH, Busa E, Albert M, Dieterich M, Haselgrove C, et al. Whole Brain Segmentation: Neurotechnique Automated Labeling of NeuroanatomicalStructures in the Human Brain. Neuron. 2002;33(3):341–355. doi:10.1016/S0896-6273(02)00569-X.

23. Wang B, Zhu J, Pierson E, Ramazzotti D, Batzoglou S. Visualization and analysis of single-cell rna-seq data by kernel-based similarity learning. Nature Methods. 2017;14(4):414–416. doi:10.1038/nMeth.4207.

24. Lihi, Zelnik-manor L, Perona P, Perona P. Self-tuning spectral clustering. Advances in Neural Information Processing Systems 17. 2004;2:1601–1608. doi:10.1.1.84.7940.

25. Van Der Maaten L, Hinton G. Visualizing Data using t-SNE. Journal of Machine Learning Research. 2008;9:2579–2605.

26. Good P. Permutation tests: a practical guide to resampling methods for testing hypotheses. Springer New York; 2000.

27. Ovod V, Ramsey KN, Mawuenyega KG, Bollinger JG, Hicks T, Schneider T, et al. Amyloid β concentrations and stable isotope labeling kinetics of human plasma specific to central nervous system amyloidosis. Alzheimer's and Dementia. 2017;13(8):841–849. doi:10.1016/j.jalz.2017.06.2266.

28. Nakamura A, Kaneko N, Villemagne VL, Kato T, Doecke J, Doré V, et al. High performance plasma amyloid-β biomarkers for Alzheimer's disease. Nature. 2018;554(7691):249–254. doi:10.1038/nature25456.

29. Gupta VB, Doecke JD, Hone E, Pedrini S, Laws SM, Thambisetty M, et al. Plasma apolipoprotein J as a potential biomarker for Alzheimer's disease: Australian Imaging, Biomarkers and Lifestyle study of aging. Alzheimer's & Dementia: Diagnosis, Assessment & Disease Monitoring. 2016;3:18–26. doi:10.1016/j.dadm.2015.12.001.

30. Lövheim H, Elgh F, Johansson A, Zetterberg H, Blennow K, Hallmans G, et al. Plasma concentrations of free amyloid β cannot predict the development of Alzheimer's disease. Alzheimer's and Dementia. 2017;13(7):778–782. doi:10.1016/j.jalz.2016.12.004.

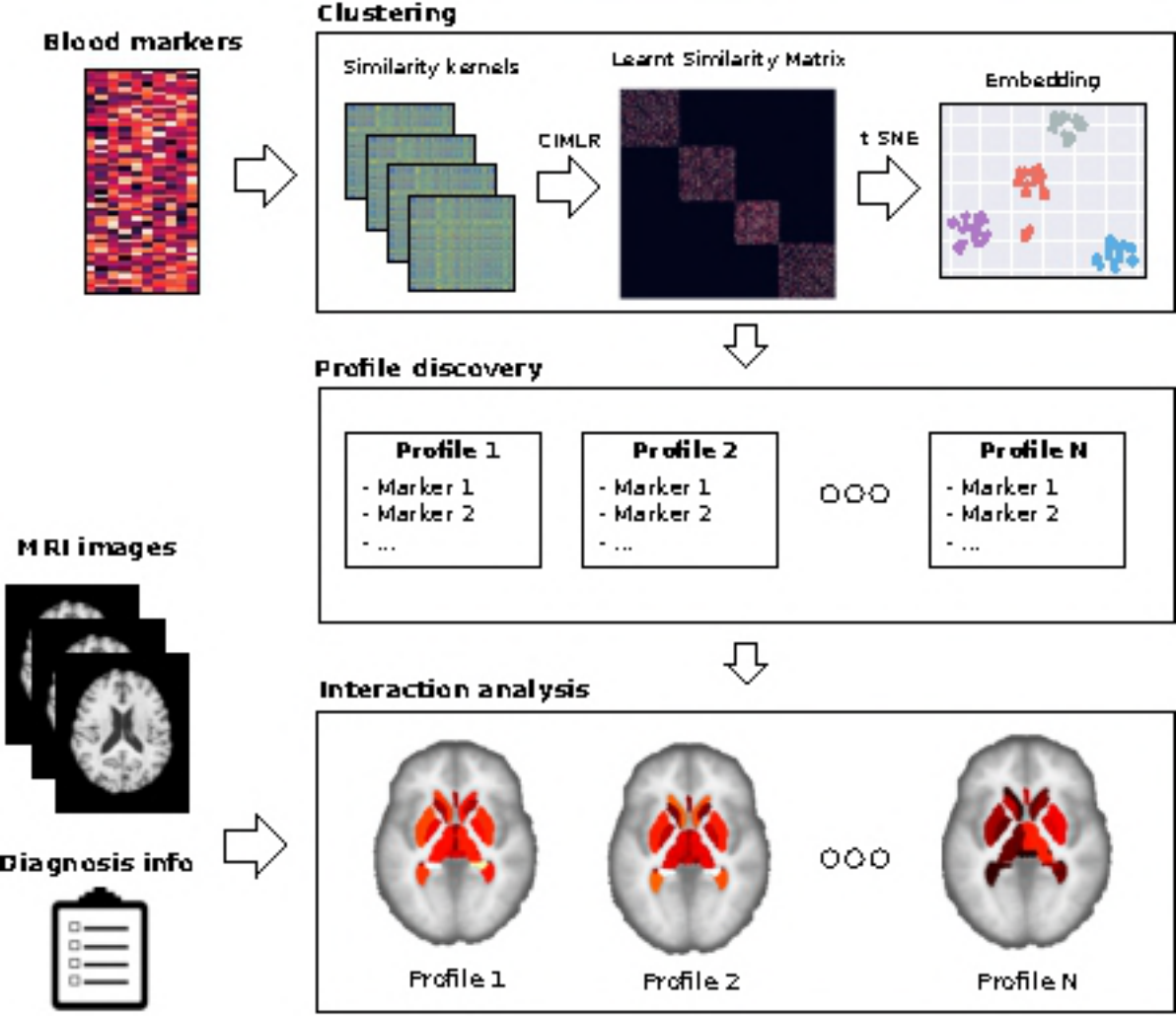
Blood markers
Clustering
Similarity kernels
CIMLR
Learnt Similarity Matrix
t SNE
Embedding
Profile discovery
Profile 1
- Marker 1
- Marker 2
- ...
Profile 2
- Marker 1
- Marker 2
- ...
Profile N
- Marker 1
- Marker 2
- ...
MRI images
Diagnosis info
Interaction analysis
Profile 1
Profile 2
Profile N

	CN - C1 vs RAGE	MCI - C1 vs RAGE	AD - C1 vs RAGE	CN - C2 vs RAGE	MCI - C2 vs RAGE	AD - C2 vs RAGE	CN - C3 vs RAGE	MCI - C3 vs RAGE	AD - C3 vs RAGE	CN - C4 vs RAGE	MCI - C4 vs RAGE	AD - C4 vs RAGE
Left-Lateral-Ventricle	0.13	0.27	0.89	0.51	0.76	0.76	0.41	0.15	0.62	0.9	1	1
Left-Inf-Lat-Vent	0.029	0.55	0.065	0.36	0.28	0.29	0.1	0.039	0.93	0.98	0.87	0.34
Left-Cerebellum-White-Matter	0.74	0.22	0.63	0.92	0.69	0.3	0.49	0.48	0.55	0.18	0.031	0.9
Left-Cerebellum-Cortex	0.008	0.66	0.95	0.16	0.078	0.82	0.66	0.56	0.44	0.037	0.069	0.39
Left-Thalamus-Proper	0.46	0.57	0.94	0.96	0.78	0.48	0.86	0.049	0.64	0.43	0.35	0.85
Left-Caudate	0.31	0.54	0.62	0.36	0.27	0.25	0.061	0.48	0.32	0.81	0.36	0.73
Left-Putamen	0.19	0.081	0.039	1	0.32	0.38	0.2	0.38	0.93	0.89	0.91	0.21
Left-Pallidum	0.048	0.58	0.07	0.5	0.46	0.46	0.074	0.41	0.38	0.24	0.35	0.66
3rd-Ventricle	0.34	0.77	0.23	0.41	0.25	0.17	0.6	0.12	0.39	0.7	0.97	0.47
4th-Ventricle	0.092	0.39	0.14	0.36	0.007	0.18	0.51	0.69	0.47	0.072	0.13	0.34
Brain-Stem	0.42	0.19	0.51	0.26	0.61	0.83	0.5	0.82	0.75	0.62	0.07	0.8
Left-Hippocampus	0.002	0.12	0.74	0.021	0.6	0.7	0.63	0.055	0.65	0.4	0.38	0.75
Left-Amygdala	0.079	0.11	0.82	0.97	0.51	0.34	0.59	0.09	0.2	0.084	0.41	0.95
CSF	0.096	0.07	0.19	1	0.19	0.95	0.75	0.75	0.57	0.062	0.96	0.047
Left-Accumbens-area	0.32	0.088	0.62	0.37	0.71	0.36	0.72	0.37	0.063	0.84	0.71	0.16
Left-VentralDC	0.49	0.4	0.91	0.77	0.39	0.92	0.91	0.042	0.8	0.19	0.066	0.99
Left-vessel	0.071	0.81	0.26	0.054	0.078	0.32	0.87	0.8	0.92	0.94	0.12	0.65
Left-choroid-plexus	0.15	0.13	0.39	0.22	0.56	0.69	0.91	0.019	0.85	0.78	0.96	0.67
Right-Lateral-Ventricle	0.044	0.3	0.89	0.46	0.81	0.92	0.24	0.52	0.43	0.84	0.56	0.64
Right-Inf-Lat-Vent	0.022	0.79	0.052	0.24	0.8	1	0.33	0.14	0.41	0.82	0.41	0.16
Right-Cerebellum-White-Matter	0.54	0.56	0.95	0.81	0.07	0.88	0.61	0.54	0.72	0.091	0.007	0.83
Right-Cerebellum-Cortex	0.013	0.86	0.81	0.32	0.045	0.91	0.7	0.53	0.34	0.025	0.01	0.49
Right-Thalamus-Proper	0.36	0.63	0.71	0.5	0.9	0.74	0.58	0.16	0.43	0.33	0.37	0.98
Right-Caudate	0.69	0.35	0.84	0.19	0.73	0.37	0.13	0.99	0.65	0.68	0.64	0.82
Right-Putamen	0.52	0.1	0.25	0.5	0.97	0.24	0.24	0.17	0.78	0.74	0.8	0.95
Right-Pallidum	0.96	0.93	0.14	0.046	0.65	0.21	0.21	0.4	0.94	0.36	0.84	0.65
Right-Hippocampus	0.004	0.34	0.88	0.011	0.39	0.64	0.82	0.17	0.9	0.41	0.23	0.43
Right-Amygdala	0.22	0.081	0.67	0.88	0.95	0.16	1	0.069	0.49	0.17	0.92	0.86
Right-Accumbens-area	0.008	0.77	0.066	0.14	0.8	0.21	0.55	0.77	0.74	0.4	0.8	0.22
Right-VentralDC	0.23	0.63	0.57	0.9	0.21	0.85	0.92	0.12	0.63	0.24	0.031	0.99
Right-vessel	0.036	0.02	0.061	0.23	0.24	0.42	0.36	0.11	0.16	0.87	0.096	1
Right-choroid-plexus	0.53	0.79	0.23	0.78	0.021	0.55	0.83	0.14	1	0.51	0.52	0.46
WM-hypointensities	0.046	0.46	0.94	0.47	0.61	0.037	0.32	0.21	0.95	0.008	0.4	0.05
Optic-Chiasm	0.74	0.45	0.83	0.28	0.38	0.52	0.84	0.4	0.03	0.53	0.43	0.11
CC_Posterior	0.46	0.37	0.68	0.29	0.9	0.14	0.35	0.74	0.52	0.23	0.72	0.7
CC_Mid_Posterior	0.11	0.12	0.84	0.36	0.03	0.7	0.016	0.068	0.75	0.71	0.41	0.88
CC_Central	0.007	0.2	0.43	0.98	0.72	0.63	0.006	0.82	0.23	0.75	0.61	0.48
CC_Mid_Anterior	0.063	0.49	0.83	0.53	0.75	0.61	0.023	0.4	0.064	0.53	0.92	0.056
CC_Anterior	0.31	0.2	0.04	0.11	0.87	0.064	0.36	0.69	0.28	0.021	0.19	0.73

$p < 0.05$
$p < 0.01$
$p < 0.001$

	C1 - CN vs AD	C2 - CN vs AD	C3 - CN vs AD	C4 - CN vs AD	C1 - CN vs MCI	C2 - CN vs MCI	C3 - CN vs MCI	C4 - CN vs MCI	C1 - MCI vs AD	C2 - MCI vs AD	C3 - MCI vs AD	C4 - MCI vs AD
Left-Lateral-Ventricle	0.89	0.094	0.73	0.02	0.31	0.5	0.61	0.053	0.91	0.075	0.68	0.28
Left-Inf-Lat-Vent	0.75	0.65	0.4	0.057	0.41	0.92	0.072	0.061	0.8	0.24	0.9	0.26
Left-Cerebellum-White-Matter	0.81	0.25	0.9	0.69	0.78	0.33	0.89	0.3	0.76	0.51	0.73	0.42
Left-Cerebellum-Cortex	0.51	0.86	0.25	0.8	0.46	0.84	0.25	0.38	0.84	0.44	0.67	0.26
Left-Thalamus-Proper	0.92	0.27	0.3	0.19	0.88	0.33	0.14	0.26	0.91	0.66	0.95	0.69
Left-Caudate	0.92	0.29	0.79	0.73	0.74	0.084	0.89	0.53	0.53	0.61	0.83	0.57
Left-Putamen	0.67	0.21	0.45	0.55	0.57	0.088	0.65	0.39	0.49	0.77	0.38	0.86
Left-Pallidum	0.2	0.009	0.69	0.42	0.16	0.16	0.88	0.91	0.81	0.36	0.67	0.11
3rd-Ventricle	0.77	0.79	0.14	0.011	0.84	0.31	0.062	0.018	0.87	0.13	0.73	0.34
4th-Ventricle	0.089	0.31	0.17	0.89	0.12	0.56	0.2	0.76	1	0.17	0.97	0.75
Brain-Stem	0.41	0.039	0.64	0.89	0.38	0.36	0.93	0.38	0.6	0.26	0.22	0.16
Left-Hippocampus	0.73	0.12	0.5	0.86	0.24	0.62	0.23	0.66	0.48	0.24	0.8	0.6
Left-Amygdala	0.78	0.26	0.1	0.82	0.86	0.26	0.33	0.55	0.093	0.6	0.5	0.85
CSF	0.089	0.92	0.4	0.36	0.091	0.75	0.41	0.62	0.4	0.38	0.29	0.22
Left-Accumbens-area	0.73	0.25	0.53	0.53	0.48	0.095	0.21	0.96	0.86	0.88	0.92	0.056
Left-VentralDC	0.49	0.38	0.54	0.53	0.71	0.44	0.36	0.42	0.33	0.5	0.77	0.93
Left-vessel	0.05	0.14	0.42	0.48	0.001	0.74	0.67	0.2	0.38	0.022	0.36	0.71
Left-choroid-plexus	0.67	0.43	0.36	0.002	0.87	0.46	0.2	0.28	0.22	0.67	0.91	0.015
Right-Lateral-Ventricle	0.82	0.38	0.63	0.078	0.25	0.65	0.53	0.11	0.99	0.24	0.56	0.19
Right-Inf-Lat-Vent	0.51	0.39	0.51	0.2	0.53	0.87	0.095	0.18	0.45	0.29	0.86	0.48
Right-Cerebellum-White-Matter	0.57	0.17	0.51	0.9	0.88	0.14	0.77	0.87	0.65	0.78	0.2	0.8
Right-Cerebellum-Cortex	0.37	0.93	0.28	0.82	0.36	0.83	0.34	0.59	0.93	0.59	0.53	0.7
Right-Thalamus-Proper	0.85	0.24	0.32	0.22	0.53	0.54	0.51	0.18	0.51	0.41	0.24	0.63
Right-Caudate	0.76	0.45	0.9	0.86	0.46	0.15	0.74	0.84	0.39	0.32	0.32	0.61
Right-Putamen	0.55	0.34	0.61	0.5	0.25	0.23	0.78	0.27	0.49	0.48	0.21	0.83
Right-Pallidum	0.34	0.02	0.84	0.79	0.15	0.11	0.72	0.78	0.36	0.36	1	0.3
Right-Hippocampus	0.7	0.072	0.45	0.66	0.46	0.35	0.47	0.51	0.22	0.28	0.74	0.8
Right-Amygdala	0.78	0.27	0.2	0.51	0.87	0.37	0.35	0.24	0.12	0.58	0.35	0.91
Right-Accumbens-area	0.81	0.36	0.32	0.55	0.74	0.11	0.31	0.76	0.92	0.28	1	0.61
Right-VentralDC	0.59	0.56	0.43	0.57	0.61	0.64	0.38	0.26	0.37	0.52	0.69	0.84
Right-vessel	0.51	0.87	0.58	1	0.64	0.59	0.31	0.18	0.74	0.53	0.8	0.17
Right-choroid-plexus	0.5	0.15	0.71	0.042	0.41	0.74	0.87	0.41	0.81	0.24	0.79	0.04
WM-hypointensities	0.48	0.07	0.93	0.29	0.16	0.18	0.43	0.33	0.88	0.14	0.49	0.51
Optic-Chiasm	0.75	0.74	0.8	0.031	0.29	0.27	0.96	0.37	0.035	0.17	0.69	0.18
CC_Posterior	0.62	0.98	0.53	0.2	0.93	0.31	0.043	0.7	0.27	0.4	0.48	0.13
CC_Mid_Posterior	0.82	0.62	0.92	0.001	0.8	0.38	0.52	0.042	0.51	0.7	0.3	0.12
CC_Central	0.92	0.2	0.8	0.014	0.73	0.41	0.55	0.077	0.8	0.39	0.67	0.2
CC_Mid_Anterior	0.73	0.53	0.42	0.003	0.85	0.13	0.5	0.05	0.87	0.36	0.75	0.29
CC_Anterior	0.48	1	0.25	0.33	0.74	1	0.013	0.45	0.51	0.86	0.69	0.76

$p < 0.05$
$p < 0.01$
$p < 0.001$

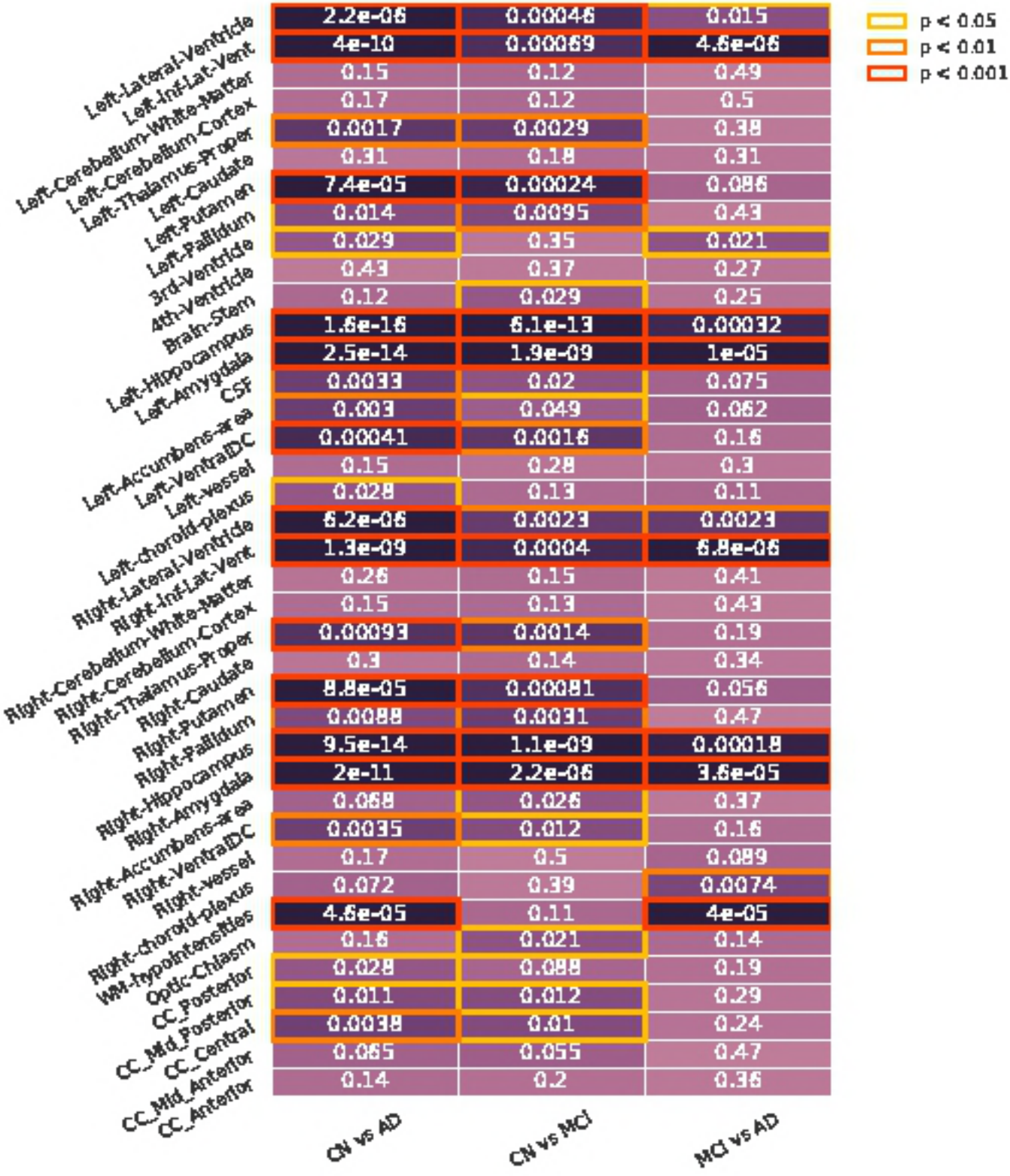
p < 0.05
p < 0.01
p < 0.001
Left-Lateral-Ventricle 2.2e-06 0.00046 0.015
Left-Inf-Lat-Vent 4e-10 0.00069 4.6e-06
Left-Cerebellum-White-Matter 0.15 0.12 0.49
Left-Cerebellum-Cortex 0.17 0.12 0.5
Left-Thalamus-Proper 0.0017 0.0029 0.38
Left-Caudate 0.31 0.18 0.31
Left-Putamen 7.4e-05 0.00024 0.086
Left-Pallidum 0.014 0.0095 0.43
3rd-Ventricle 0.029 0.35 0.021
4th-Ventricle 0.43 0.37 0.27
Brain-Stem 0.12 0.029 0.25
Left-Hippocampus 1.6e-16 6.1e-13 0.00032
Left-Amygdala 2.5e-14 1.9e-09 1e-05
CSF 0.0033 0.02 0.075
Left-Accumbens-area 0.003 0.049 0.062
Left-VentralDC 0.00041 0.0016 0.16
Left-vessel 0.15 0.28 0.3
Left-choroid-plexus 0.028 0.13 0.11
Right-Lateral-Ventricle 6.2e-06 0.0023 0.0023
Right-Inf-Lat-Vent 1.3e-09 0.0004 6.8e-06
Right-Cerebellum-White-Matter 0.26 0.15 0.41
Right-Cerebellum-Cortex 0.15 0.13 0.43
Right-Thalamus-Proper 0.00093 0.0014 0.19
Right-Caudate 0.3 0.14 0.34
Right-Putamen 8.8e-05 0.00081 0.056
Right-Pallidum 0.0088 0.0031 0.47
Right-Hippocampus 9.5e-14 1.1e-09 0.00018
Right-Amygdala 2e-11 2.2e-06 3.6e-05
Right-Accumbens-area 0.068 0.026 0.37
Right-VentralDC 0.0035 0.012 0.16
Right-vessel 0.17 0.5 0.089
Right-choroid-plexus 0.072 0.39 0.0074
WM-hypointensities 4.6e-05 0.11 4e-05
Optic-Chiasm 0.16 0.021 0.14
CC_Posterior 0.028 0.088 0.19
CC_Mid_Posterior 0.011 0.012 0.29
CC_Central 0.0038 0.01 0.24
CC_Mid_Anterior 0.065 0.055 0.47
CC_Anterior 0.14 0.2 0.36
CN vs AD
CN vs MCI
MCI vs AD

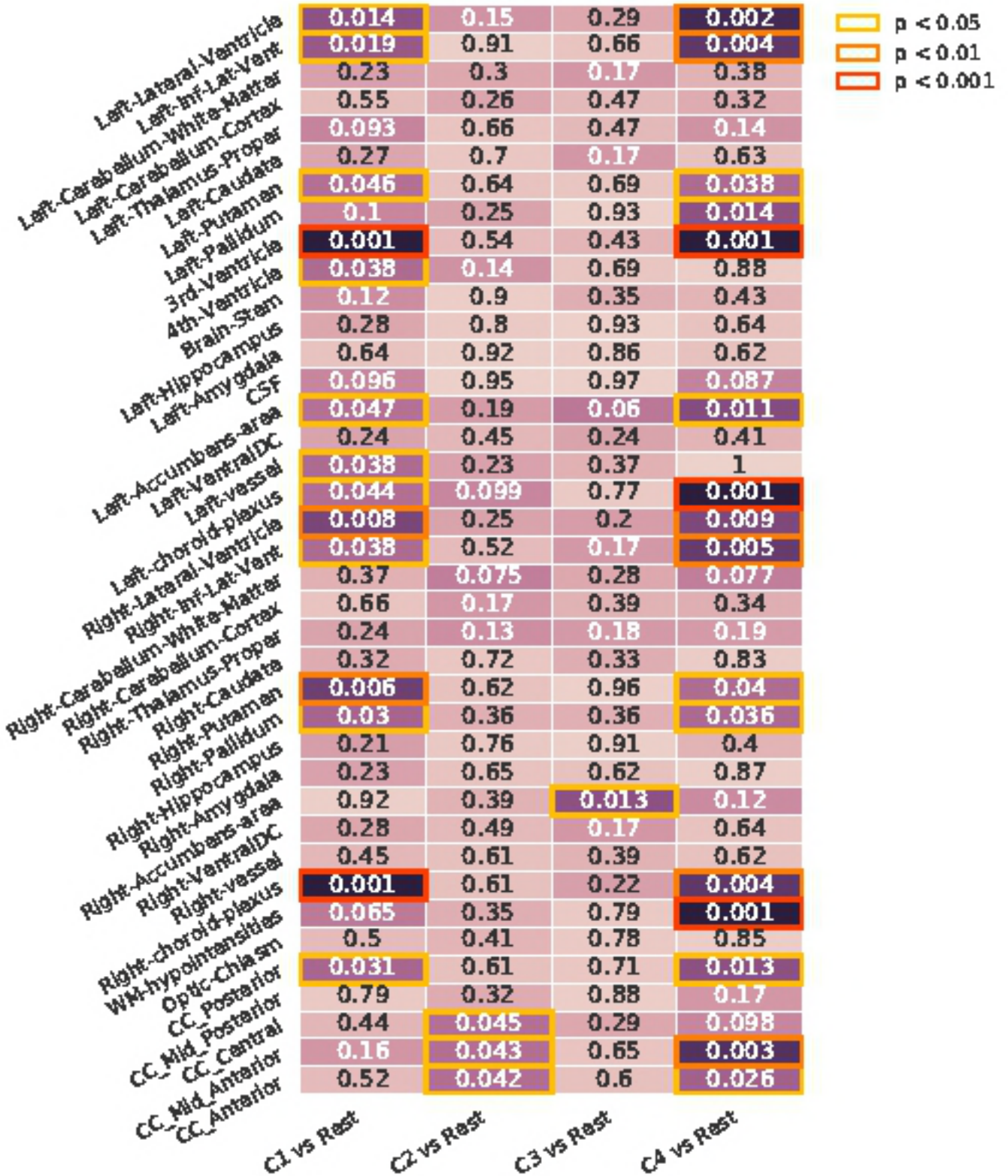
Left-Lateral-Ventricle 0.014 0.15 0.29 0.002
Left-Inf-Lat-Vent 0.019 0.91 0.66 0.004
Left-Cerebellum-White-Matter 0.23 0.3 0.17 0.38
Left-Cerebellum-Cortex 0.55 0.26 0.47 0.32
Left-Thalamus-Proper 0.093 0.66 0.47 0.14
Left-Caudate 0.27 0.7 0.17 0.63
Left-Putamen 0.046 0.64 0.69 0.038
Left-Pallidum 0.1 0.25 0.93 0.014
3rd-Ventricle 0.001 0.54 0.43 0.001
4th-Ventricle 0.038 0.14 0.69 0.88
Brain-Stem 0.12 0.9 0.35 0.43
Left-Hippocampus 0.28 0.8 0.93 0.64
Left-Amygdala 0.64 0.92 0.86 0.62
CSF 0.096 0.95 0.97 0.087
Left-Accumbens-area 0.047 0.19 0.06 0.011
Left-VentralDC 0.24 0.45 0.24 0.41
Left-vessel 0.038 0.23 0.37 1
Left-choroid-plexus 0.044 0.099 0.77 0.001
Right-Lateral-Ventricle 0.008 0.25 0.2 0.009
Right-Inf-Lat-Vent 0.038 0.52 0.17 0.005
Right-Cerebellum-White-Matter 0.37 0.075 0.28 0.077
Right-Cerebellum-Cortex 0.66 0.17 0.39 0.34
Right-Thalamus-Proper 0.24 0.13 0.18 0.19
Right-Caudate 0.32 0.72 0.33 0.83
Right-Putamen 0.006 0.62 0.96 0.04
Right-Pallidum 0.03 0.36 0.36 0.036
Right-Hippocampus 0.21 0.76 0.91 0.4
Right-Amygdala 0.23 0.65 0.62 0.87
Right-Accumbens-area 0.92 0.39 0.013 0.12
Right-VentralDC 0.28 0.49 0.17 0.64
Right-vessel 0.45 0.61 0.39 0.62
Right-choroid-plexus 0.001 0.61 0.22 0.004
WM-hypointensities 0.065 0.35 0.79 0.001
Optic-Chiasm 0.5 0.41 0.78 0.85
CC_Posterior 0.031 0.61 0.71 0.013
CC_Mid_Posterior 0.79 0.32 0.88 0.17
CC_Central 0.44 0.045 0.29 0.098
CC_Mid_Anterior 0.16 0.043 0.65 0.003
CC_Anterior 0.52 0.042 0.6 0.026
C1 vs Rest
C2 vs Rest
C3 vs Rest
C4 vs Rest
p < 0.05
p < 0.01
p < 0.001

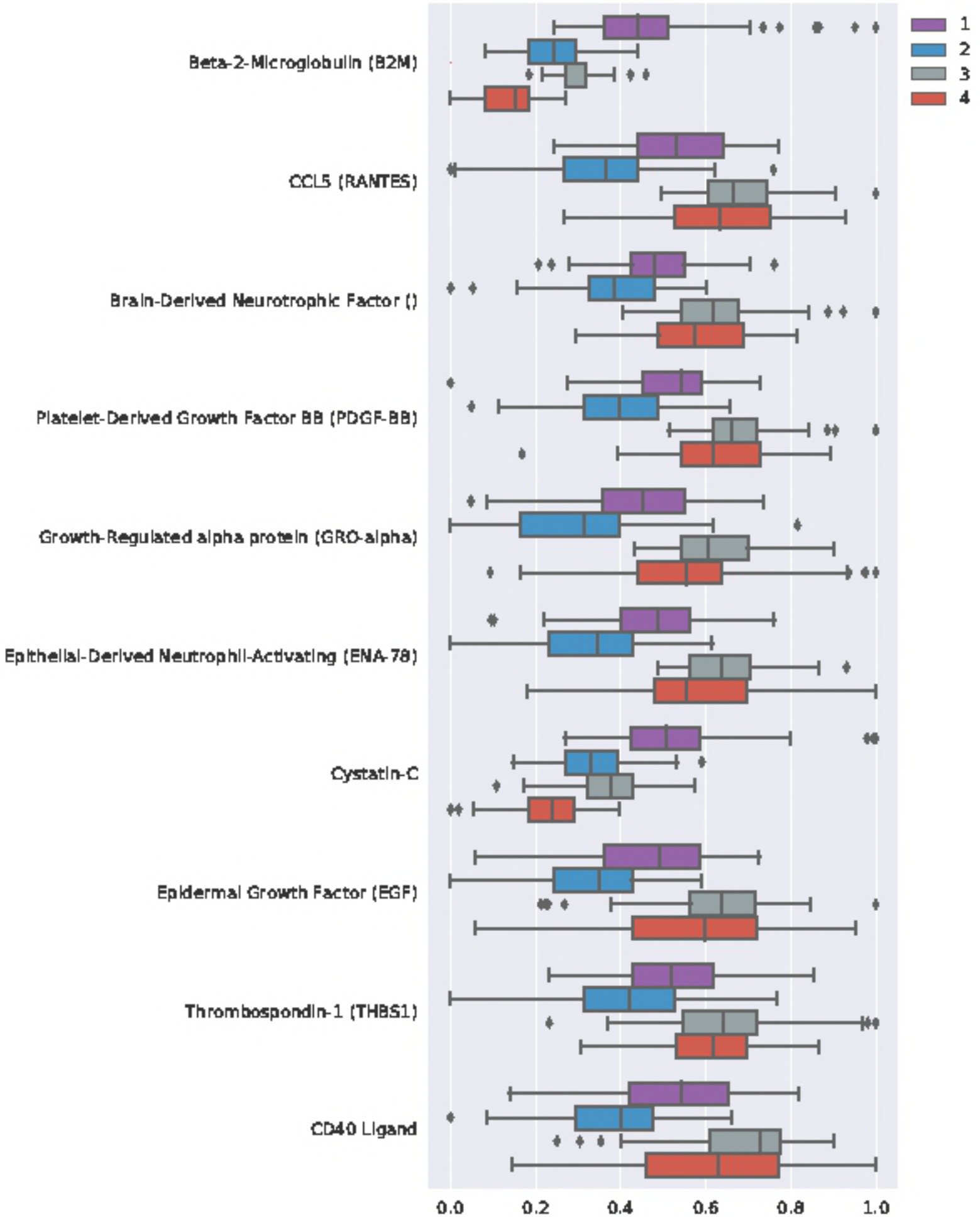
Beta-2-Microglobulin (B2M)
CCL5 (RANTES)
Brain-Derived Neurotrophic Factor ()
Platelet-Derived Growth Factor BB (PDGF-BB)
Growth-Regulated alpha protein (GRO-alpha)
Epithelial-Derived Neutrophil-Activating (ENA-78)
Cystatin-C
Epidermal Growth Factor (EGF)
Thrombospondin-1 (THBS1)
CD40 Ligand
0.0
0.2
0.4
0.6
0.8
1.0
1
2
3
4

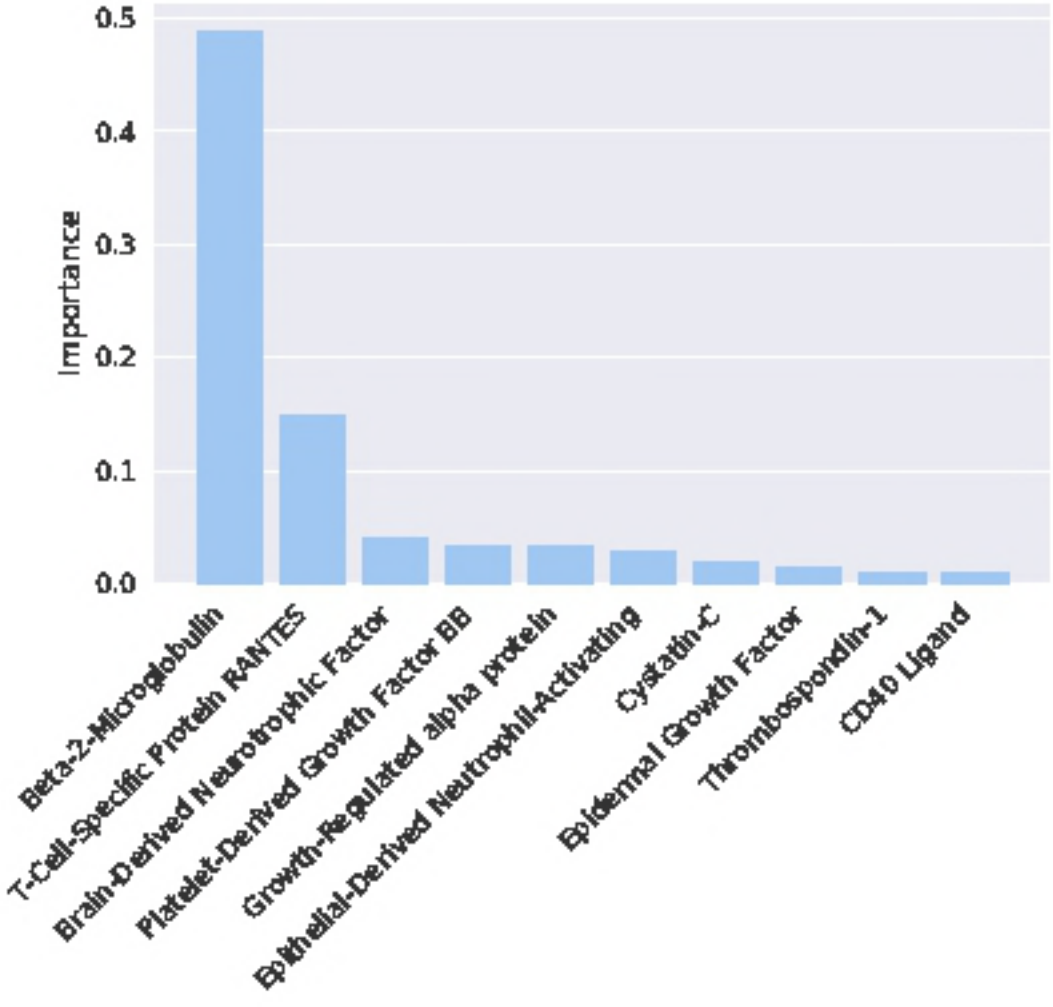
Importance
0.5
0.4
0.3
0.2
0.1
0.0
Beta-2-Microglobulin
T-Cell-Specific Protein RANTES
Brain-Derived Neurotrophic Factor
Platelet-Derived Growth Factor BB
Growth-Regulated alpha protein
Epithelial-Derived Neutrophil-Activating
Cystatin-C
Epidermal Growth Factor
Thrombospondin-1
CD40 Ligand

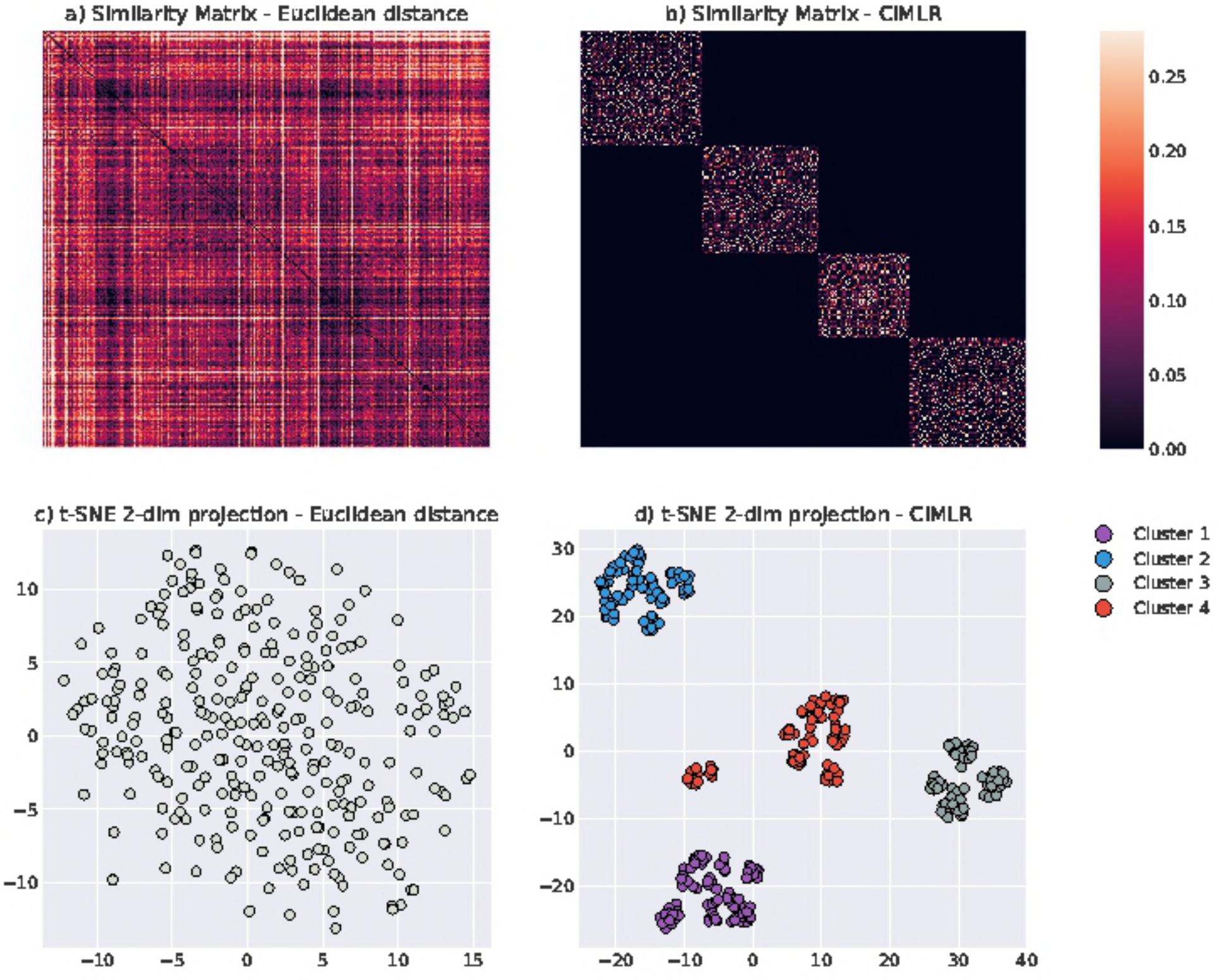
a) Similarity Matrix - Euclidean distance
b) Similarity Matrix - CIMLR
0.25
0.20
0.15
0.10
0.05
0.00
c) t-SNE 2-dim projection - Euclidean distance
d) t-SNE 2-dim projection - CIMLR
Cluster 1
Cluster 2
Cluster 3
Cluster 4

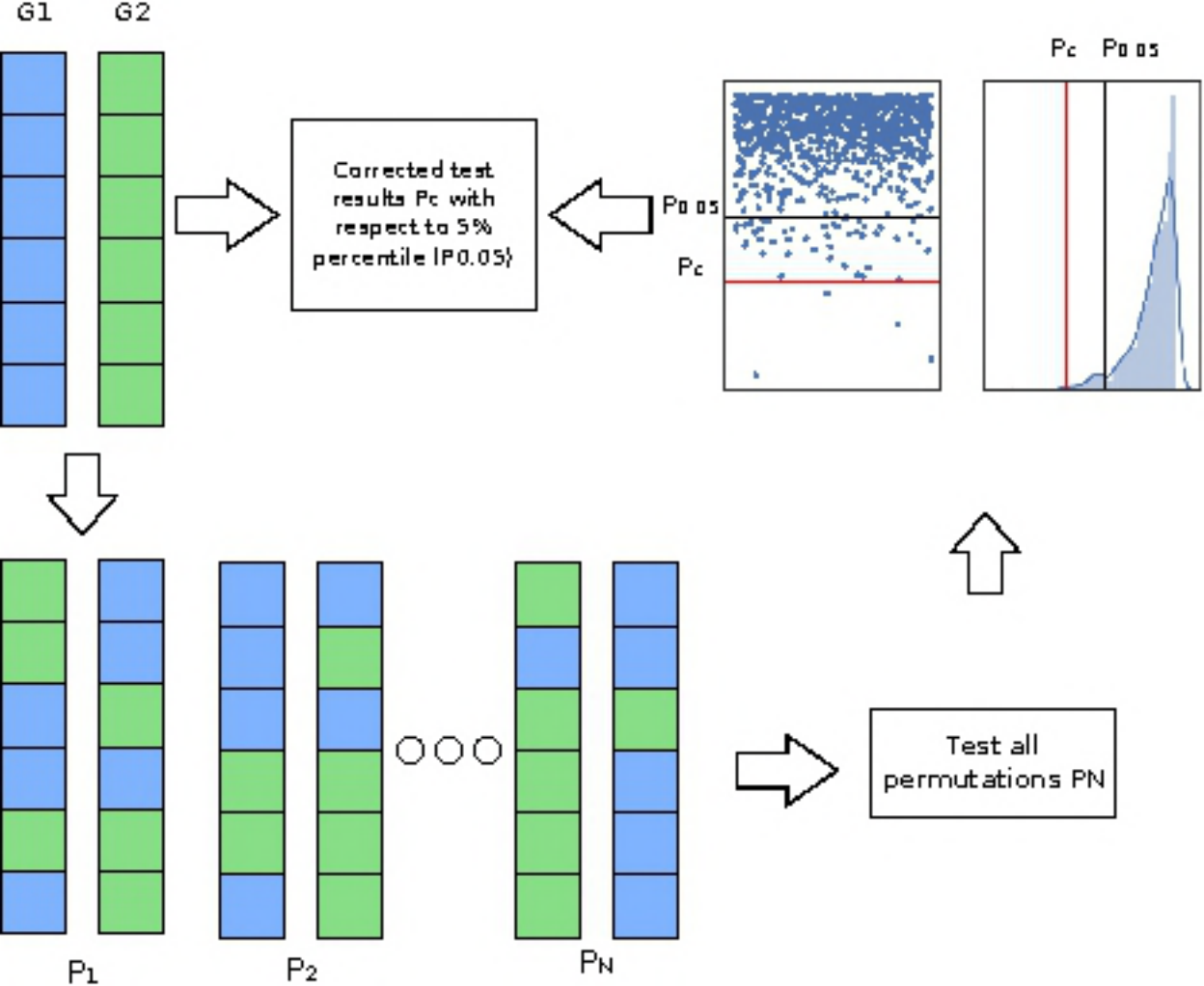
G1
G2
Corrected test results Pc with respect to 5% percentile (P0.05)
P0.05
Pc
Pc
P0.05
Test all permutations PN
P1
P2
PN